Synthesis and Structural Characterization of Lanthanide-Containing Polytungsto-antimonate [Sb 3 (μ 3 -O) 2 Ln(H 2 O)Ln(H 2 O) 2 2 (SbW 10 O 37) 2 (SbW 8 O 31) 2] 22 - Molecules Deriving from the Decomposition of the [Sb 8 W 36 O 132] 24 - Macroanion

Maxime Dufaye, Sylvain Duval, Gregory Stoclet, Dimitrije Mara, Rik van Deun, Thierry Loiseau

Synthesis and structural characterization of a series of lanthanide-containing polytungsto-antimonate $[\{Sb_3(\mu^3\text{-}O)_2Ln(H_2O)Ln(H_2O)_2\}_2(SbW_{10}O_{37})_2(SbW_8O_{31})_2]^{22-}$ (Ln = Gd, Tb, Dy, Ho, Er, Tm, Yb, Lu) molecules deriving from the decomposition of the $[Sb_8W_{36}O_{132}]^{24-}$ macroanion.

Dr. Maxime Dufaye,[†] Dr. Sylvain Duval,[†,*] Dr. Gregory Stoclet,[‡] Dimitrije Mara,[§] Prof. Dr. Rik Van Deun,[§] and Dr. Thierry Loiseau[†]

Contribution from [†]Unité de Catalyse et Chimie du Solide (UCCS) – UMR CNRS 8181, Université de Lille, Centrale Lille, Univ. Artois, F-59000 Lille, France, [‡]Unité Matériaux Et Transformations (UMET) – UMR CNRS 8207, Université de Lille, Centrale Lille, F-59000 Lille, France and [§]Luminescent Lanthanide Lab (L^3), Department of Chemistry, Ghent University, Krijgslaan 281, S3, 9000 Ghent, Belgium.

[*] To whom correspondence should be addressed. E-mail: sylvain.duval@univ-lille.fr. Phone: (33) 3 20 434 973, Fax: (33) 3 20 43 48 95.
http://uccs.univ-lille1.fr/index.php/fr/annuaire/289-duval-sylvain

Abstract: Reaction of the tungsto-antimonate $[Sb_8W_{36}O_{132}]^{24-}$ polyoxometalate with late trivalent lanthanide cations (from Gd to Lu) gives rise to the formation of eight isostructural molecular compounds $[\{Sb_3(\mu^3\text{-}O)_2Ln(H_2O)Ln(H_2O)_2(SbW_{10}O_{37})(SbW_8O_{31})\}_2]^{22-}$ (Ln = Gd^{III} (**1**), Tb^{III} (**2**), Dy^{III} (**3**), Ho^{III} (**4**), Er^{III} (**5**), Tm^{III} (**6**), Yb^{III} (**7**), Lu^{III} (**8**)). All compounds were characterized by routine solid-state techniques (IR spectroscopy, TGA, single crystal X-ray diffraction) and, by SAXS measurements in aqueous solutions to assess their stabilities. Luminescent properties of compounds **5** and **7** were also studied.

Keywords: polyoxometalates, single-crystal X-ray diffraction, lanthanides, luminescence, SAXS.

Introduction.

Polyoxometalates are a versatile class of inorganic molecules built up from the condensation, mainly through oxolation or olation reactions of metallic cations in their higher oxidation state (V^V, Mo^{VI}, W^{VI}, …). These metalates can either auto-assemble to form species of the isopolyanion type or can assemble around a tetra- or tricoordinated templating agent, which is generally coming from the *p* group elements (P^V, Si^{IV}, $As^{III/V}$, $Sb^{III/V}$, Bi^{III}, …) to generate a molecular system from the heteropolyanion series. Most of these compounds have the ability to sustain a partial hydrolysis, leading to the formation of lacunary species. It then becomes easy to incorporate a large group of transition heterometals within these newly formed vacancies to finely tune the chemical properties and potential applications of this family of materials.[1–9] In addition to these properties, some lacunary polyanions are able to be further condensed to produce macrocyclic entities exhibiting a cryptand like behavior. For instance, the trilacunary $[B\text{-}\alpha\text{-}AsW_9O_{33}]^{9-}$ and the hexalacunary $[P_2W_{12}O_{48}]^{14-}$ species can be assembled to form the $[As_4W_{40}O_{140}]^{28-}$ and the $[P_8W_{48}O_{184}]^{40-}$ molecules, respectively.[10,11] The use of these cryptand-like inorganic polyoxometallic molecules has successfully led to the incorporation of various transition metals and, more recently of actinide elements through the work of Pope, Kortz and Abramov and in our research group.[12–16] In the latter context, it is known that some highly radiotoxic trivalent actinides can be surrogated by trivalent lanthanide cations. As a general way, the approach consisting in using lanthanide cations associated to polyanionic moieties is not new and, some spectacular compounds were described during the last two decades.[17–20] As such, one may quote the pioneering work of M. T. Pope *et al.* in 1997, [21] who were able to synthesize the biggest polytungstate $[As_{12}Ce^{III}_{16}(H_2O)_{36}W_{148}O_{524}]^{76-}$ to date by making use of cerium(III) cations with $[AsW_9O_{33}]^{9-}$ and free $[WO_4]^{2-}$. Several research groups continued exploring this topic and were able to produce very large Ln^{III}-POM assemblies. For instance, G. R. Patzke *et al.* could obtain the very large polyanionic architectures $[Gd_8As_{12}W_{124}O_{432}(H_2O)_{22}]^{60-}$, $[Cs\square Ln_6As_6W_{63}O_{218}(H_2O)_{14}(OH)_4]^{25-}$ and $[Ln_{16}As_{16}W_{164}O_{576}(OH)_8(H_2O)_{42}]^{80-}$ making use of arsenicotungstic precursors associated with mid and late lanthanide centres (Eu^{III}, Gd^{III}, Tb^{III}, Dy^{III}, Ho^{III}, Er^{III}). [22–24] Hill and Yamaze also described interesting assemblies containing lanthanides.[25,26] An interesting review about polyoxometalates with lanthanide elements was also written by Kortz *et al.* few years ago.[27]

Considering the results based on the aforementioned cryptands and the use of lanthanides with polyanions, we were interested in the use of another related anionic cryptand-like molecule, $[Na_2Sb_8W_{36}O_{132}(H_2O)_4]^{22-}$, constructed around the condensation of four [B-β-$SbW_9O_{33}]^{9-}$ trilacunary units and four $\{Sb^{III}O_4\}$ groups. In the solid state, this cryptand is interacting with two sodium cations and four water molecules located in its vicinity. Within the $[Na_2Sb_8W_{36}O_{132}(H_2O)_4]^{22-}$ cryptand, we have attempted the possibility to substitute the alkali elements by trivalent lanthanides, potentially simulating the crystal-chemical behavior of trivalent actinide elements. Related work on antimonytungstate polyanions was performed a few years ago by Zang and co-workers. They have reported several closely related architectures constructed by the reaction of the trivacant $[SbW_9O_{33}]^{9-}$ unit with La^{III}, Pr^{III}, Tb^{III}, Dy^{III} and Ho^{III}.[28]

In this work, we report on the synthesis of eight isostructural molecular entities $[\{Sb_3(\mu^3\text{-}O)_2Ln(H_2O)Ln(H_2O)_2(SbW_{10}O_{37})(SbW_8O_{31})\}_2]^{22-}$, resulting from the synthetic combination of the anionic $[Na_2Sb_8W_{36}O_{132}(H_2O)_4]^{22-}$ precursor with a series of eight heavy trivalent lanthanide cations from gadolinium(III) to lutetium(III) (Ln^{III} = Gd^{III} (**1**), Tb^{III} (**2**), Dy^{III} (**3**), Ho^{III} (**4**), Er^{III} (**5**), Tm^{III} (**6**), Yb^{III} (**7**), Lu^{III} (**8**)). The single-crystal XRD analysis revealed that the original arrangement of the polytungsto-antimonate is not preserved during the aqueous reactions, giving rise to a new set of polyanionic arrangements of $[SbW_{10}O_{37}]^{11-}$ together with $[SbW_8O_{31}]^{11-}$ moieties. This contribution deals with the synthetic procedure, X-ray diffraction and IR characterizations, thermogravimetric analyses and SAXS investigations of this new molecular species $[\{Sb_3(\mu^3\text{-}O)_2Ln(H_2O)Ln(H_2O)_2(SbW_{10}O_{37})(SbW_8O_{31})\}_2]^{22-}$. Luminescence properties have been studied for the samples incorporating Er(III) and Yb(III) elements.

Synthesis discussion. A close look at the $\{Sb_8^{III}W_{36}O_{132}\}$ polyanion shows that it differs from the related $\{As_4^{III}W_{40}O_{140}\}$ cryptand (Figure 1), which has been previously studied in our research group.[29]

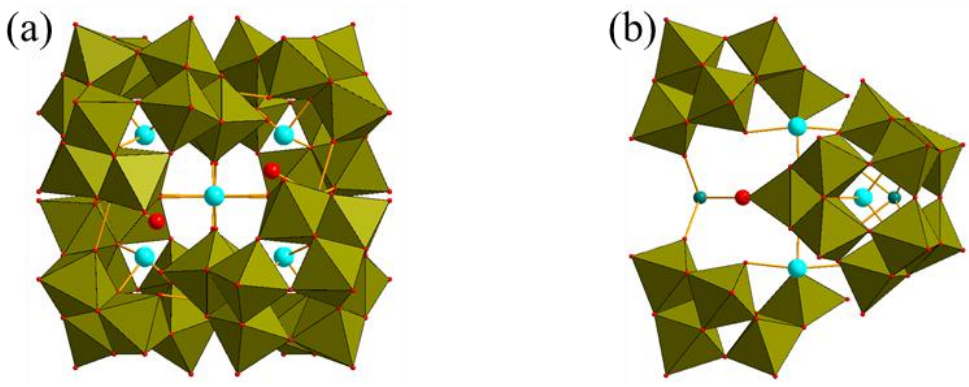

Figure 1: (a) Front and (b) side views of the structural representation of the $\{Sb_8W_{36}O_{132}\}$ precursor. Green octahedron: $\{WO_6\}$; blue spheres: Sb atoms; dark green spheres: Na atoms; red spheres: O atoms.

On the one hand, the arsenicotungstic $\{As_4W_{40}O_{140}\}$ compound displays two different complexation sites: one S1 site is located at the center of the molecule, suitable for the complexation of alkali or alkaline-earth cations and four S2 coordination sites better adapted for the complexation of transition metal cations. On the other hand, the antimonytungstic $\{Sb_8W_{36}O_{132}\}$ molecule stabilizes only two peripheral sodium cations, pointing toward its center. Each sodium cation interacts with the oxo groups from the vacancies of two $[B\text{-}\beta\text{-}SbW_9O_{33}]^{9-}$ sub-units (distance Na-O = 2.442 Å) and two water molecules located in the cavity (distance Na-OH_2 = 2.450 Å). This specific polytungsto-antimonate macromolecule seems to have been peculiarly less investigated for the complexation of transition metals [30] and, as far as we known, no direct incorporation of only lanthanide cations has been yet reported in the literature. In our synthesis route, two molar equivalents of lanthanides were added in aqueous solution to one $\{Sb_8W_{36}O_{132}\}$ moiety. The reaction has been carried out in the presence of formate species acting as condensation modulators, by trying to substitute the two originally trapped sodium cations by lanthanide cations. Surprisingly, this synthetic approach only led to the formation of a new molecular system clearly identified for the eight later trivalent lanthanide cations ($Gd^{III} \rightarrow Lu^{III}$). These various synthesis batches gave rise to the appearance of crystalline compounds mainly with needle-like shapes, some of them are characterized by crystals containing cavities (Figure S1). Based on the X-ray diffraction analyses (see below for more details), it was also revealed that the molecular architecture of the original cryptand molecule was not maintained, but was reorganized to generate two distinct polyanionic moieties (Figure 2).

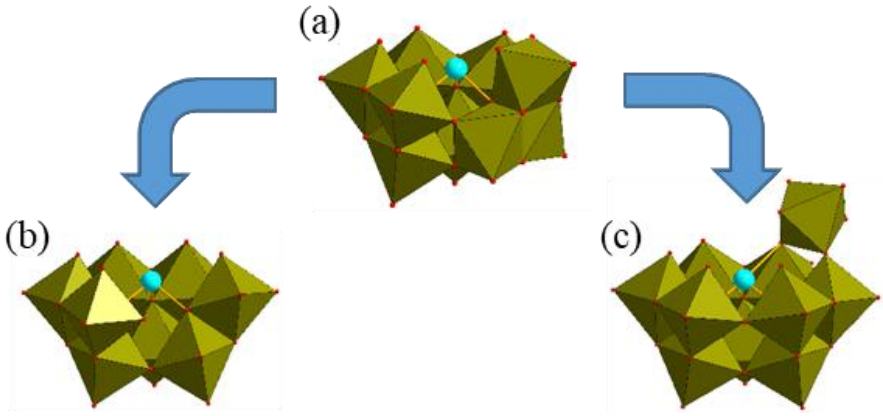

Figure 2: (a) Structural representation of the $\{B\text{-}\beta\text{-}SbW_9O_{34}\}$ sub-unit precursor and the rearrangement moieties $\{\alpha\text{-}SbW_8O_{31}\}$ (b) and $\{\alpha\text{-}SbW_{10}O_{37}\}$ (c), occurring in the eight compounds, when associated with lanthanide cations ($Gd^{III} \rightarrow Lu^{III}$).

Indeed, the $[B\text{-}\beta\text{-}Sb^{III}W_9O_{33}]^{9-}$ sub-units of the cryptand-like $\{Sb_8W_{36}O_{132}\}$ species, are reorganized in $\{\alpha\text{-}Sb^{III}W_8O_{31}\}$ and $\{\alpha\text{-}Sb^{III}W_{10}O_{37}\}$ antimony-polytungstate blocks and the additional antimonate $\{Sb_3{}^{III}O_7\}$ block, in which the trivalent oxidation state of the central antimony atoms is preserved.

The use of six light lanthanides ($La^{III} \rightarrow Nd^{III}$, Sm^{III}, Eu^{III}) in combination with the $\{Sb_8W_{36}O_{132}\}$ species, never generated such a polyanionic arrangement since only metatungstate $[NaW_{12}O_{40}]^{7-}$ crystals were sometimes produced. The rest of the time, only amorphous powders were precipitated.

These observations highlight two interesting points for our synthetic route:

(i) the macromolecule $\{Sb_8W_{36}O_{132}\}$ may be not stable as the cryptand architecture is not kept.

(ii) the size of the lanthanide cation used in the synthesis appears to play a drastic role as large ionic radii lanthanides (> 1.06 Å i.e Eu^{III}) could not be incorporated.

Structural description. The X-ray diffraction structure determination of compounds **1**-**8** reveals that they all crystallize in the triclinic *P*-1 space group, except for compound **4** (with Ho^{III}) crystallizing in the monoclinic $P2_1/n$ space group. Nevertheless, the eight molecular entities are isostructural with a general formula $[\{Sb_3(\mu^3\text{-}O)_2Ln(H_2O)Ln(H_2O)_2(SbW_{10}O_{37})(SbW_8O_{31})\}_2]^{22-}$ (with Ln^{III} = Gd^{III} (**1**), Tb^{III} (**2**), Dy^{III} (**3**), Ho^{III} (**4**), Er^{III} (**5**), Tm^{III} (**6**), Yb^{III} (**7**), Lu^{III} (**8**)) for the anionic moiety. They are constructed by the complex association of several different building blocks. The asymmetric unit is composed of one $[SbW_8O_{31}]^{11-}$ motif, one $[SbW_{10}O_{37}]^{11-}$ motif, one trinuclear antimony-centered $\{Sb_3O_7\}$ motif and two independent lanthanide cations as discrete units, with an eight-fold coordination describing a typical bicapped trigonal prismatic environment. The lanthanide centers coordination spheres exhibit two different compositions, $LnO_6(H_2O)_2$ and $LnO_7(H_2O)$. The complete molecular entity is obtained by application of an inversion center located on its geometric center and results in an "S" shaped molecule (Figure 3a). The two $[SbW_8O_{31}]^{11-}$ moieties are close to the geometric center of the molecule while the two $[SbW_{10}O_{37}]^{11-}$ units are located at the periphery. Within these two distinct entities, the Sb atoms are three-fold coordinated with typical Sb-O distances ranging between 1.95 Å to 2 Å. In the same way, two lanthanide cations (i.e. $LnO_7(H_2O)$) appear to be closer to the inversion centers (Ln_{int}) while the two others (i.e. $LnO_6(H_2O)_2$) are off-centered (Ln_{ext}) (Figure 3b).

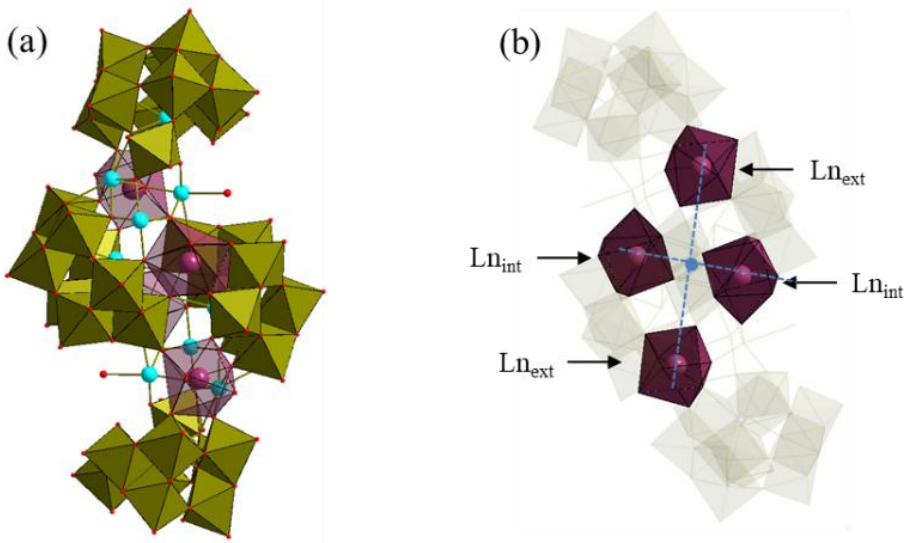

Figure 3: (a) Structural representation of the molecular anionic $[\{Sb_3(\mu^3\text{-}O)_2Ln(H_2O)Ln(H_2O)_2(SbW_{10}O_{37})(SbW_8O_{31})\}_2]^{22-}$ entity in compounds (**1**-**8**) and (b) localization of the so-called internal and external lanthanide centers. Green octahedron: $\{WO_6\}$; violet bicapped trigonal prism: $\{LnO_8\}$; blue spheres: Sb atoms.

In the anionic polyoxometalate **1**-**8** species, the Ln_{int} centers are interacting with the two $\{SbW_8O_{31}\}$ units through six Ln-O bonds. Five of them possess typical distances for lanthanide-O_{POM} interactions comprised between 2.200(18) Å and 2.453(9) Å through the series $Gd^{III} \rightarrow Lu^{III}$. The last oxygen atom interacts through much longer Ln-O bond distances of 2.70(2) (in **1**) Å towards 2.655(12) Å (in **8**). This is probably due to the fact that this oxygen atom also interacts with the central Sb heteroelement of the $\{SbW_8O_{31}\}$ unit. The coordination sphere of the Ln_{int} centers is completed by one μ^3-O bridge (Ln_{int}-O bond distance = 2.504(9) Å (in **1**) – 2.399(10) Å (in **8**)) linking two Sb atoms of the $\{Sb_3O_7\}$ unit and one terminal water molecule (Ln-OH_2 bond distance = 2.466(9) Å (in **1**) - 2.373(10) Å (in **8**)). The external lanthanides cations Ln_{ext} interact with one type of $\{SbW_8O_{31}\}$ polyanion through two oxygen atoms of its vacancy (Ln-O bond distance = 2.384(9) Å and 2.284(8) (in **1**) to 2.238(9) and 2.312(11) Å (in **8**)) and with the second type $\{SbW_8O_{31}\}$ unit through only one oxygen atom (Ln-O bond distance = 2.337(9) Å (in **1**) to 2.261(11) Å (in **8**)). The coordination sphere of these centers is completed by two oxygen atoms coming from the $\{SbW_{10}O_{37}\}$ moiety (Ln-O bond distance from 2.343(9) Å to 2.451(9) (in **1**) and 2.268(9) Å to 2.385(11) (in **8**)), one μ^3-O bridge linking two Sb centers of the $\{Sb_3O_7\}$ unit (Ln-O bond distance = 2.463(9) (in **1**) Å to 2.402(9) Å (in **8**)) and two terminal water molecules (average Ln-O bond distances from 2.434(10) (in **1**) Å to 2.338(11) Å (in **8**)) (Figure 4).

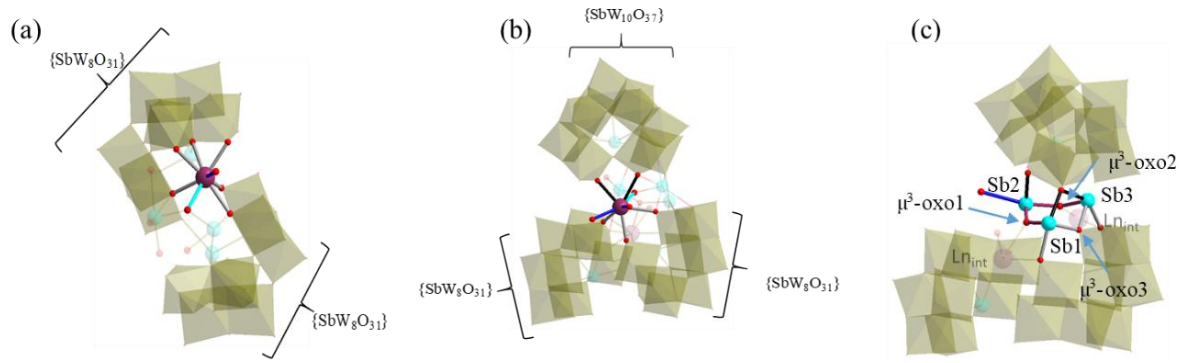

Figure 4: (a) and (b) Structural representation of the external and internal lanthanide coordination environment. (c) Environment of the $\{Sb_3O_7\}$ unit.

In this series of systems, an interesting observation is the presence of the trimeric $\{Sb_3O_7\}$ entity, in which Sb centers possess a four-fold coordination (trigonal bipyramidal geometry if one considers the occurrence of a non-bonding lone pair of the AX_4E-type) and a calculated bond valence sum of III (See Table S2). For this trinuclear block, the Sb-O distances are longer (on average 2.1 Å, with variations from 1.96 Å up to 2.56 Å) than the ones observed for the Sb-O bonds (typically around 1.95 Å to 2 Å) from the three-fold coordinated Sb centers located within the polyanionic $[SbW_8O_{31}]^{11-}$ and $[SbW_{10}O_{37}]^{11-}$ motifs of the molecules. This $\{Sb_3O_7\}$ fragment comes from the decomposition of the initial precursor, which releases free Sb atoms, undergoing a reorganization and oxo-condensation process. It seems to play a role in stabilizing the arrangement of the polyoxometalate molecule since it interacts with both $\{SbW_8O_{31}\}$ and $\{SbW_{10}O_{37}\}$ sub-units and the two types of lanthanide centers.

A close examination at the Ln-O distances in the series of compounds (**1**-**8**) shows that they are correlated to the decrease of the ionic radii of the lanthanides when going from gadolinium to lutetium (See Figure 5). Nevertheless, we can notice that this decrease is not constant along the series. It could eventually be explained by differences in the data quality of the X-ray diffraction analyses, for which the R_{int} parameters vary widely from 5.25% for compound **6** to 14.88% for compound **3**.

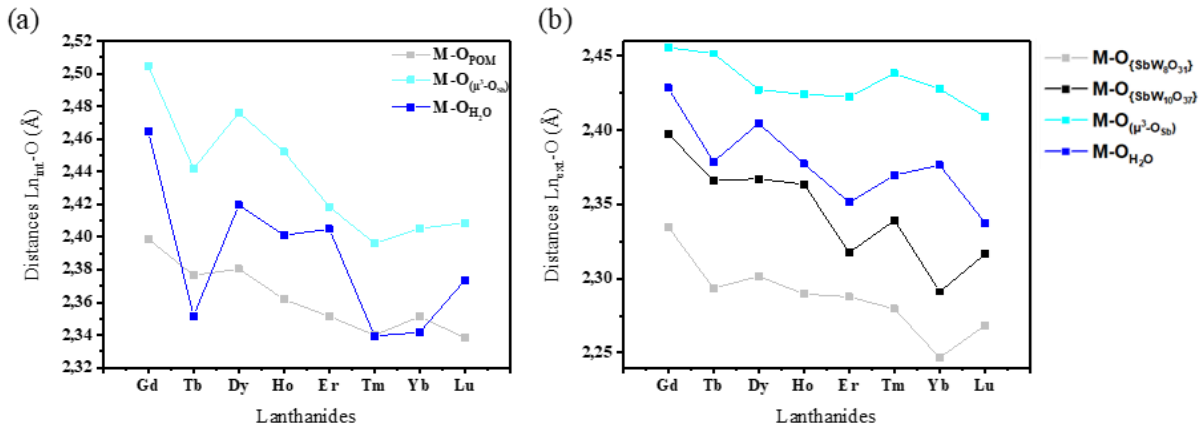

Figure 5: Comparison of Ln_{int}-O average distances (a) and Ln_{ext}-O average distances (b) in compounds **1-8** highlighting the global decrease following the lanthanide contraction of the series.

As explained above, we could only obtain successful results using the eight later lanthanide cations $Gd^{III} \rightarrow Lu^{III}$. All the syntheses performed using the lightest lanthanide elements ($La^{III} \rightarrow Nd^{III}$, Sm^{III}, Eu^{III}) only gave rise to the formation of crystals of the original $\{Sb_8W_{36}O_{132}\}$ precursor or a metatungstate $\{NaW_{12}O_{40}\}$-based solid. This interesting point can be correlated to the ionic radius of the lanthanide cations along the series. Indeed, the variation (about more than 15%)[31] between the lanthanum cation (1.16 Å) and the lutetium cation (0.977 Å) could explain why larger lanthanide centers could not be incorporated in this recomposed molecular architecture, since it requires an eight-fold coordinated unit, whereas a nine-fold coordination environment is most often expected for the lightest lanthanides. Lanthanide(III) cations are peculiarly interesting as they can serve as surrogates for actinide(III) crystal-chemical behavior. A comparison of the ionic radii of trivalent lanthanides with some tri- or tetra-valent actinides is shown in Figure 6.

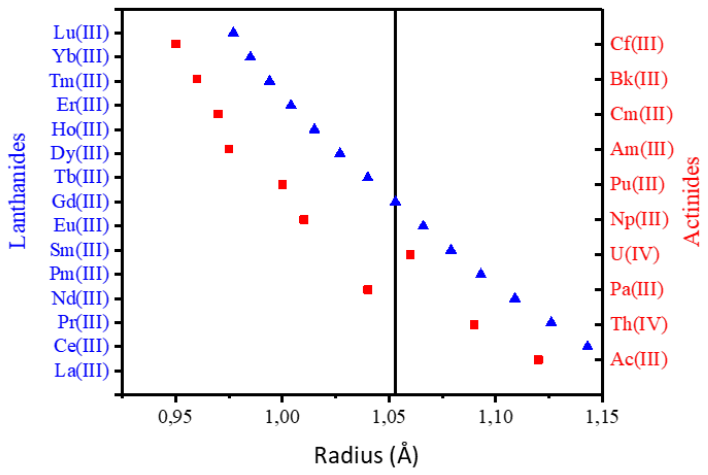

Figure 6: Comparison of Ln^{III} ionic radii with some An^{III} and An^{IV} cations.[31] Blue triangles represent the lanthanide series and the red squares the actinide series.

From the X-ray diffraction analyses, we can observe that the upper limit is found for gadolinium(IIII) (ionic radius = 1.06 Å). By comparison with the trivalent or tetravalent actinide elements, we might suggest that the several trivalent cations from protactinium(III) to californium(III), could effectively be incorporated in the present molecular architecture, using the synthetic approach presented in this work.

The charge balance of the polyanionic $[\{Sb_3(\mu^3\text{-}O)_2Ln(H_2O)Ln(H_2O)_2(SbW_{10}O_{37})(SbW_8O_{31})\}_2]^{22-}$ moiety is ensured by the occurrence of sodium cations and in some cases, by different contents of tetramethylammonium cations. For the latter, they were undoubtedly located from X-ray diffraction analyses for compound **5**, whereas only an infrared signature is observed for compounds **1**-**5** and **7** (typical vibration bands at 1490 cm^{-1} and 1350 cm^{-1}; Figure S3). The presence of these alkylammonium cations comes from the initial $\{Sb_8W_{36}O_{132}\}$ precursor. The sodium cations are either located from X-ray diffraction techniques or determined by elemental analyses in order to balance the 22 negative charges of the polyanionic moiety. For compounds **6** and **8**, only sodium counter-cations are present.

As mentioned in the introduction, the literature related to previously reported lanthanide antimony-tungstate polyanions reveals that the compounds **1**-**8** are structurally close to the results described by Zang *et al.*[28] In their work, they reported several antimony-tungstate polyanions containing lanthanides starting from the $Na_9[B\text{-}\alpha\text{-}SbW_9O_{33}]$ polyoxometalate. Three of the reported molecules with Tb^{III}, Dy^{III} and Ho^{III} are similar to those of the present work. They were synthesized by a complex synthetic pathway implying the use of the aforementioned lanthanides with the addition of 2-picolinic acid and of the $[SbW_9O_{33}]^{9-}$ precursor, following by addition of a 1M HCl solution containing Sb_2O_3. pH adjustment at 6.5 was then performed and LiCl added, resulting in the crystallization of colorless product after three days. This approach differs from ours as we did use sodium formate instead of 2-picolinic acid and the $\{Sb_8W_{36}O_{132}\}$ macromolecule instead of the $[SbW_9O_{33}]^{9-}$ precursor. It seems that our method is more direct in obtaining this structural archetype even if both kinds of precursors seems to decompose and reorganize to form the "S" shape title molecules.

The main structural difference with our molecules is the occurrence of picolinate ligands, which contribute to the coordination environments of the two external lanthanide cations (Ln_{ext}), whereas terminal water molecules were found in compounds **1**-**8**. All the Sb-O and Ln-O distances reported by *Zang et al.* are also similar to the ones observed in compounds **1**-**8**.

Thermal behaviour. Thermogravimetric analyses were performed to determine the water content of the crystalline phases **1**-**8** (Figure S2). Calculations were based on the observation of the first weight loss up to the first plateau (i.e. 200°C for all compounds). The amounts of water molecules related to the $[\{Sb_3(\mu^3\text{-}O)_2Ln(H_2O)Ln(H_2O)_2(SbW_{10}O_{37})(SbW_8O_{31})\}_2]^{22-}$ formula were 64 (obs.: 9.8 %) for **1**, 54 (obs.: 8 %) for **2**, 61 (obs.: 9.1 %) for **3**, 63 (obs.: 9.3 %) for **4**, 38 (obs.: 5.8 %) for **5**, 52 (obs.: 7.7 %) for **6**, 42 (obs.: 6.3 %) for **7** and 42 (obs.: 6.3 %) for **8**.

For each thermogravimetric measurement, the curve goes up from 550°C, until 800°C. This related weight gain is about 1.4 %, corresponding to ca. 148 g.mol^{-1}. It was assigned to the oxidation of the ten Sb^{III} cations (incorporated in compounds **1-8**), into {Sb^{V}-O} groups with the corresponding uptake of one oxygen atom (from the air atmosphere) per antimony center following (Eq. 1) below.

$$\text{(Eq. 1)} \qquad 5\ Sb_2{}^{III}O_3 \rightarrow \ 5\ Sb_2{}^{V}O_5$$

The uptake of 10 oxygen atoms (ca. 160 g.mol^{-1}) is closely related to the 1.4% / 148 g.mol^{-1} of the weight gain.

Infrared spectroscopy. The IR spectra of compounds **1-8** are shown in Figure S3 and were compared to those of the initial {SbW_9O_{33}} and {$Sb_8W_{36}O_{132}$} precursors. Reports of the wavenumber values of the W-O and W-O-W vibrations related to the polyanion backbone are gathered in Table S3. We notice that all the compounds **1-8** exhibit an identical signature in the 1100-400 cm^{-1} range corresponding to the polyanionic species. This observation indicates all compounds have the same polyanionic backbone as was observed from the X-ray diffraction analyses. Furthermore, the presence of tetramethylammonium cations can be seen in most IR spectra (range 1490 cm^{-1} - 1350 cm^{-1}) and was further clearly revealed from the X-ray diffraction analyses of compound **5**. As explained above, they come from the {$Sb_8W_{36}O_{132}$} precursors synthesized using these counter-cations. Nevertheless, they were not visible for the other single-crystal XRD structures, maybe due to disorder of these organic cations with sodium cations and solvent water molecules.

Luminescence measurements.

The emission intensities were limited due to the inefficiency of the charge transfer (CT) from O-Sb or O-W bonds to excite the accepting levels of the lanthanide cations and, in addition, to the quenching effect of the water molecules bound to lanthanide cations in their coordination sphere. Indeed, we could only compare the luminescence properties of compound **5** containing erbium(III) and compound **7** containing ytterbium(III), for which excitation and emission spectra were recorded (Figure 7). In the excitation spectrum of erbium(III), two bands can be observed at 366 nm and 525 nm. The first one being really weak, sample **5** has been excited at 525 nm, corresponding to the f-f transitions $^4S_{3/2} \leftarrow {}^4I_{15/2}$ and $^2H_{11/2} \leftarrow {}^4I_{15/2}$ to obtain an emission peak at 1540 nm corresponding to the transition $^4I_{13/2} \rightarrow {}^4I_{15/2}$. A similar measurement was performed for the ytterbium(III)-containing compound **7**. Only one band can be seen at 360 nm in the excitation spectrum. Excitation in this band gives an emission peak centered around 1000 nm, showing a splitting at 980 nm and 1120 nm (due to the stark effect) corresponding to the $^2F_{5/2} \rightarrow {}^2F_{7/2}$ transition. The decay profiles of the two compounds **5** and **7** were measured as well and the luminescence lifetimes could be determined. For the erbium-containing compound **5**, the decay curve could be modelled using a biexponential function giving the lifetime τ_{av} = 1.31 ± 0.02 μs. The same was done for the ytterbium-containing molecule, giving a lifetime τ_1 = 11.2 ± 0.09 μs. The difference in the emission intensities observed for the two compounds **5** and **7** originates from the quenching effect

exerted by water molecules in the coordination sphere of the erbium and ytterbium cations. Indeed, the second overtone of the water O-H vibration is located at around 1400 nm which is close to the emission of erbium. This quenching effect is not observed for ytterbium as the emission peaks (980 nm and 1120 nm) are relatively far from the overtones of the water molecules.

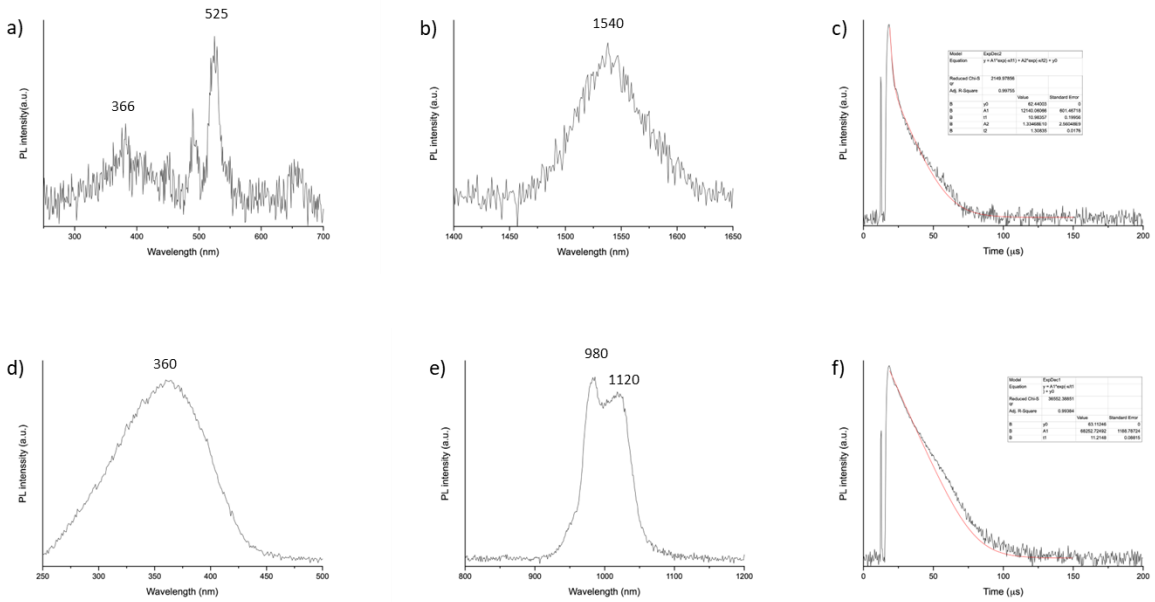

Figure 7: Excitation and emission spectra, and decay curves for the erbium-containing compound **5** (a), (b), (c) and the ytterbium-containing compound **7** (d), (e), (f).

SAXS measurements. In order to estimate the stability of the eight molecular systems in aqueous solution, we carried out Small Angle X-ray Scattering (SAXS) analysis, which has been previously reported in literature for the characterization of molecular inorganic polyoxometalate-like species.[32] The strategy lies on the dissolution of a given amount of crystalline product of the different compounds **1**-**8** in water, poured in a 1.5 mm diameter glass capillary, with the targeted concentration of 25 mmol.L^{-1}.

The modelling of the scattering curves is presented on Figure 8. In the SAXS region (i.e. for q < 0.8 $Å^{-1}$), a specific evolution can be modelled using the atomic positions coming from the single-crystal XRD model of the studied compounds. We observe a particularly good correlation of the position of the intensity decrease for all curves and specifically at around 0.2 $Å^{-1}$ < q < 0.4 $Å^{-1}$. This indicates that the geometrical parameters and structural size determined from XRD measurements are maintained in solution. A gyration radius (*R*g) was calculated (using a cylindrical model) for the molecules at a value of 13.1 Å. These values are in good agreement with the cylindrical dimensions of the molecules, extracted form XRD analyses, showing a length of 27 Å with a width of 16 Å (which makes a radius ranging from 8 Å to 13.5 Å) (Figure 8). Therefore, the anionic species $[\{Sb_3(\mu^3\text{-}O)_2Ln(H_2O)Ln(H_2O)_2(SbW_{10}O_{37})(SbW_8O_{31})\}_2]^{22-}$ through the series of lanthanide Gd^{III} →

Lu^{III} preserves their structural integrity in aqueous solution after their dissolution, and no aggregation process seems to occur.

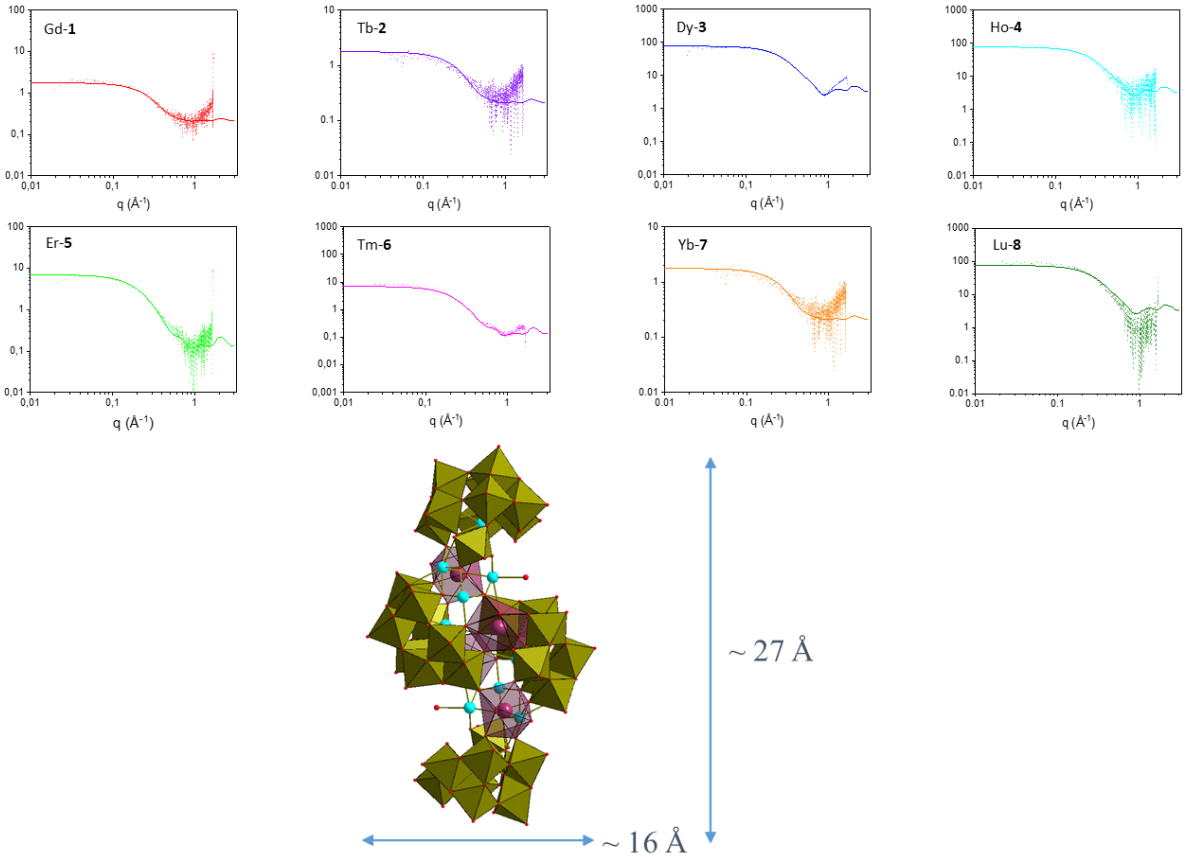

Figure 8: Simulation (full line) using SolX of the X-ray scattering curves (dotted lines) of compounds **1-8**. Below, geometrical parameters of the molecular compound considering a cylindrical model.

Conclusion.

We have made use of the $[Sb_8W_{36}O_{132}]^{24-}$ macromolecule to bind trivalent cations from the second part of the lanthanide series ($Gd^{III} \rightarrow Lu^{III}$). When associated to these elements, it appears that the macroanion architecture is not maintained but rather decomposed in two polyanionic sub-units, $[SbW_8O_{31}]^{11-}$ and $[SbW_{10}O_{37}]^{11-}$, forming an isostructural "S" shaped molecule, in which four single lanthanide centers are incorporated. These lanthanide elements interact with both polyanionic moieties and also with a trinuclear $\{Sb_3O_7\}$ sub-group giving a structural cohesion to an anionic elongated anionic molecule $[\{Sb_3(\mu^3\text{-}O)_2Ln(H_2O)Ln(H_2O)_2(SbW_{10}O_{37})(SbW_8O_{31})\}_2]^{22-}$. Solution studies by small angle X-ray scattering indicate that these molecules are stable upon redissolution in aqueous solutions and no aggregation process seems to occur. The comparison of the ionic radii of the inserted lanthanide centers with some trivalent actinide elements seems to indicate the possibility to incorporate them in this solution-stable architecture. Furthermore, the presence of two labile

water molecules on the external lanthanide centers could open a way for further modification of these molecules by adding organic linkers, e.g. to synthesize POMOF materials, as it was emphasized by Zang *et al.* work.

Experimental section.

Synthesis

The compounds (**1**-**8**) have been synthesized using the following lanthanide sources without any further purification: gadolinium nitrate hexahydrate ($Gd(NO_3)_3{\cdot}6H_2O$, Aldrich, 99.9%), terbium chloride hexahydrate ($TbCl_3{\cdot}6H_2O$, Aldrich, 99.9%), dysprosium chloride hexahydrate ($DyCl_3{\cdot}6H_2O$, Aldrich, 99.9%), holmium chloride hexahydrate ($HoCl_3{\cdot}6H_2O$, Aldrich, 99.9%), erbium nitrate hexahydrate ($Er(NO_3)_3{\cdot}6H_2O$, Aldrich, 99.9%), thulium chloride hexahydrate ($TmCl_3{\cdot}6H_2O$, Aldrich, 99.9%), ytterbium chloride hexahydrate ($YbCl_3{\cdot}6H_2O$, Aldrich, 99.9%) and lutetium chloride hexahydrate ($LuCl_3{\cdot}6H_2O$, Aldrich, 99.9%). Other chemical reactants: $Na_2WO_4{\cdot}2H_2O$ (Aldrich, 99%), Sb_2O_3 (Aldrich, 99%), $SbCl_3$ (Aldrich, 99%), $N(CH_3)_4Cl$ (Aldrich, 99%), HCOONa (Aldrich, 99%), NaCl (Aldrich, 99%).

$(N(CH_3)_4)_{10}Na_{12}[Sb_8W_{36}O_{132}(H_2O)_4]{\cdot}72H_2O$ (hereafter called $\{Sb_8W_{36}O_{132}\}$) was synthesized from the $Na_9[SbW_9O_{33}]{\cdot}12H_2O$ precursor according to a literature procedure.[33] $Na_9[SbW_9O_{33}]{\cdot}12H_2O$ was synthesized by the solubilization of $Na_2WO_4{\cdot}2H_2O$ (40 g, 0.1 mmol) and Sb_2O_3 (1.96 g, 6.7 mmol) in 10 mL of distilled water followed by HCl addition to form the $Na_9[SbW_9O_{33}]{\cdot}12H_2O$ polyoxometalate.[33] The macromolecular salt $(N(CH_3)_4)_{10}Na_{12}[Sb_8W_{36}O_{132}(H_2O)_4]{\cdot}72H_2O$ was prepared by dissolution of $SbCl_3$ (1.2 g, 5.26 mmol) in a boiling aqueous solution of the $Na_9[SbW_9O_{33}]{\cdot}12H_2O$ precursor (15.6 g, 5.24 mmol), followed by pH adjustment at 6-7 and addition of $N(CH_3)_4Cl$ (6.8 g, 62 mmol) to obtain the rapid crystallization (few hours) of the molecule. All other reagents were used without any further purifications.

$Na_{20}(N(CH_3)_4)_2[\{Sb_3(\mu^3\text{-}O)_2Gd(H_2O)Gd(H_2O)_2(SbW_{10}O_{37})(SbW_8O_{31})\}_2]{\cdot}58H_2O$ (1): $\{Sb_8W_{36}O_{132}\}$ (250 mg, 0.0254 mmol) is dissolved in 5 mL of NaCl (0.2M). $Gd(NO_3)_3{\cdot}5H_2O$ (25.4 mg, 0.0563 mmol) is added to the solution and the mixture is heated at 70°C during 20 min. HCOONa (300 mg, 4.4 mmol) is then added to the solution with gentle stirring. The solution was kept at 70°C during an additional 15 minutes and then slowly cooled to room temperature. After several days, white crystals appeared and were collected for analyses. Yield: 208 mg (83%).

IR (cm^{-1}):

1629(m), 1590(sh), 931(m), 862(sh), 767(s), 676(s), 585(s), 511(s), 422(s).

ICP-OES:

$Na_{20}(N(CH_3)_4)_2[\{Sb_3(\mu^3\text{-}O)_2Gd(H_2O)Gd(H_2O)_2(SbW_{10}O_{37})(SbW_8O_{31})\}_2]{\cdot}58H_2O$: Na (3.59%), Sb (9.5%), W (52.3%), Gd (5.26%). Calculated: Na (3.63%), Sb (9.62%), W (52.3%), Gd (4.97%).

$Na_{19}(N(CH_3)_4)_3[\{Sb_3(\mu^3\text{-}O)_2Tb(H_2O)Tb(H_2O)_2(SbW_{10}O_{37})(SbW_8O_{31})\}_2]\cdot 48H_2O$ (2): The same procedure has been used for the synthesis of compound **2** but, using $TbCl_3\cdot 6H_2O$ (33.7 mg, 0.0903 mmol) instead. Yield: 198 mg (79%).

IR (cm^{-1}):

1637(sh), 1586(m), 929(m), 854(s), 766(s), 670(s), 622(s), 422(s).

ICP-OES:

$Na_{19}(N(CH_3)_4)_3[\{Sb_3(\mu^3\text{-}O)_2Tb(H_2O)Tb(H_2O)_2(SbW_{10}O_{37})(SbW_8O_{31})\}_2]\cdot 48H_2O$: Na (3.16%), Sb (10.1%), W (53.4%), Tb (5.77%). Calculated: Na (3.57%), Sb (9.83%), W (54.1%), Tb (5.20%).

$Na_{19}(N(CH_3)_4)_3[\{Sb_3(\mu^3\text{-}O)_2Dy(H_2O)Dy(H_2O)_2(SbW_{10}O_{37})(SbW_8O_{31})\}_2]\cdot 55H_2O$ (3): The same procedure has been used for the synthesis of compound **3** but, using $DyCl_3\cdot 6H_2O$ (27.3 mg, 0.0724 mmol) instead. Yield: 214 mg (86%).

IR (cm^{-1}):

1627(m), 1588(sh), 936(m), 893(sh), 864(sh), 825(sh), 750(s), 711(s), 611(s), 425(s).

ICP-OES:

$Na_{19}(N(CH_3)_4)_3[\{Sb_3(\mu^3\text{-}O)_2Dy(H_2O)Dy(H_2O)_2(SbW_{10}O_{37})(SbW_8O_{31})\}_2]\cdot 55H_2O$: Na (3.3%), Sb (10%), W (51.8%), Dy (5.98%). Calculated: Na (3.54%), Sb (9.53%), W (53.6%), Dy (5.26%).

$Na_{18}(N(CH_3)_4)_4[\{Sb_3(\mu^3\text{-}O)_2Ho(H_2O)Ho(H_2O)_2(SbW_{10}O_{37})(SbW_8O_{31})\}_2]\cdot 57H_2O$ (4): The same procedure has been used for the synthesis of compound **4** but, using $HoCl_3\cdot 6H_2O$ (28.9 mg,0.0762 mmol) instead. Yield: 187 mg (74%).

IR (cm^{-1}):

1603(m), 930(m), 852(m), 767(s), 670(s), 616(s), 458(s), 419(s).

ICP-OES:

$Na_{18}(N(CH_3)_4)_4[\{Sb_3(\mu^3\text{-}O)_2Ho(H_2O)Ho(H_2O)_2(SbW_{10}O_{37})(SbW_8O_{31})\}_2]\cdot 57H_2O$: Na (3.05%), Sb (10.2%), W (53.8%), Ho (5.98%). Calculated: Na (3.33%), Sb (9.9%), W (53.2%), Ho (5.30%).

$Na_{21}(N(CH_3)_4)[\{Sb_3(\mu^3\text{-}O)_2Er(H_2O)Er(H_2O)_2(SbW_{10}O_{37})(SbW_8O_{31})\}_2]\cdot 32H_2O$ (5): The same procedure has been used for the synthesis of compound **5** but, using $Er(NO_3)_3\cdot 6H_2O$ (35.6 mg, 0.0772 mmol) instead. Yield: 222 mg (88%).

IR (cm^{-1}):

1627(sh), 1586(m), 931(m), 850(s), 768(s), 675(s), 589(s), 465(s), 419(s).

ICP-OES:

$Na_{21}(N(CH_3)_4)[\{Sb_3(\mu^3\text{-}O)_2Er(H_2O)Er(H_2O)_2(SbW_{10}O_{37})(SbW_8O_{31})\}_2]\cdot 32H_2O$: Na (4.54%), Sb (9.58%), W (53.1%), Er (5.75%). Calculated: Na (4.08%), Sb (9.39%), W (55.9%), Er (5.65%).

$Na_{22}[\{Sb_3(\mu^3\text{-}O)_2Tm(H_2O)Tm(H_2O)_2(SbW_{10}O_{37})(SbW_8O_{31})\}_2]\cdot 46H_2O$ (6): The same procedure has been used for the synthesis of compound **6** but, using $TmCl_3\cdot 6H_2O$ (29.2 mg,0.0762 mmol) instead. Yield: 215 mg (86%).

IR (cm^{-1}):

1623(sh), 932(m), 849(m), 808(m), 770(s), 612(s), 421(s).

ICP-OES:

$Na_{22}[\{Sb_3(\mu^3\text{-}O)_2Tm(H_2O)Tm(H_2O)_2(SbW_{10}O_{37})(SbW_8O_{31})\}_2]\cdot 46H_2O$: Na (3.91%), Sb (9.72%), W (55.2%), Tm (4.91%). Calculated: Na (4.20%), Sb (9.86%), W (55.0%), Tm (5.61%).

$Na_{21}(N(CH_3)_4)[\{Sb_3(\mu^3\text{-}O)_2Yb(H_2O)Yb(H_2O)_2(SbW_{10}O_{37})(SbW_8O_{31})\}_2]\cdot 36H_2O$ (7): The same procedure has been used for the synthesis of compound **7** but, using $YbCl_3\cdot 6H_2O$ (29.6 mg, 0.0764 mmol) instead. Yield: 199 mg (80%).

IR (cm^{-1}):

1632(sh), 1581(m), 931(m), 855(s), 811(s), 769(s), 713(s), 626(s), 469(s), 421(s).

ICP-OES:

$Na_{21}(N(CH_3)_4)[\{Sb_3(\mu^3\text{-}O)_2Yb(H_2O)Yb(H_2O)_2(SbW_{10}O_{37})(SbW_8O_{31})\}_2]\cdot 36H_2O$: Na (4.33%), Sb (10.6%), W (53.1%), Yb (5.08%). Calculated: Na (4.06%), Sb (10.2%), W (55.6%), Yb (5.81%).

$Na_{22}[\{Sb_3(\mu^3\text{-}O)_2Lu(H_2O)Lu(H_2O)_2(SbW_{10}O_{37})(SbW_8O_{31})\}_2]\cdot 36H_2O$ (8): The same procedure has been used to synthesized compound **8** but, using $LuCl_3\cdot 6H_2O$ (29.7 mg, 0.0763 mmol) instead. Yield: 187 mg (75%).

IR (cm^{-1}):

1622(m), 932(m), 853(m), 772(s), 602(s), 423(s).

ICP-OES:

$Na_{22}[\{Sb_3(\mu^3\text{-}O)_2Lu(H_2O)Lu(H_2O)_2(SbW_{10}O_{37})(SbW_8O_{31})\}_2]\cdot 36H_2O$: Na (3.76%), Sb (10.7%), W (54.9%), Lu (6.13%). Calculated: Na (4.27%), Sb (10.3%), W (55.8%), Lu (5.90%).

Single-crystal X-ray diffraction

Crystals of compounds **1-8** were selected under a polarizing optical microscope and glued on a mitegen loop for single-crystal X-ray diffraction experiments. Because of the potential instability of the crystalline network due to the loss of crystallization water from the lattice, all measurements were performed at 100K under a nitrogen flow. X-ray intensity data were collected on a Bruker X8-APEX2 CCD area-detector diffractometer using Mo-K_α radiation (λ = 0.71073 Å) with an optical fiber as collimator. Several sets of narrow data frames (10 s per frame) were collected at different values of θ for two initial values of ϕ and ω, respectively, using 0.3° increments of ϕ or ω. Data reduction was accomplished using SAINT V8.34a.[34] Due to substantial redundancy, the absorption was performed using a numerical absorption correction (SADABS 2016/3).[35] The structures were solved by direct methods, developed by successive difference Fourier syntheses, and refined by full-matrix least-squares on all F^2 data using the SHELX program suite[36] on the OLEX2 software.[37]

The final refinements included anisotropic thermal parameters of all atoms except the one that would be NPD or nearly NPD. The crystal data are given in Table S1. Supporting informations are available in CIF format.

*Specific details on the structural resolution of compound **1-8**.*

All eight structures appear to be plagued with water molecules and sodium atoms disorder which is classical in polyanions structural crystallography. When possible, these water molecules and sodium atoms were localized on the lattice but, for compounds **3**, **5**, **7** and **8**, a SQUEEZE procedure was applied using OLEX2 software to remove the weak electron densities surrounding the molecular polyoxometalate entities and the localized atoms. As a consequence, the number of cations balancing the negatively charged polyanionic units was determined using a combination of ICP-OES and EDS analyses. Explanations regarding the observed A-level and B-level alerts are available on the Checkcif of compounds **1-8** under the VRF-form.

SAXS measurements

The measurements were performed on a SAXS Xeuss 2.0 apparatus (Xenocs) equipped with a micro source using a Cu K_α radiation (λ = 1.54 Å) and point collimation (beam size: 300 x 300 μm^2). The sample to detector distance, around 35 cm, was calibrated using silver behenate as standard. Crystals of the eight compounds were dissolved in neat water. The analyzed solutions were then placed in 1.5 mm glass capillaries at a molecular concentration of about 25 mM for the anionic $[\{Sb_3(\mu^3\text{-}O)_2Ln(H_2O)Ln(H_2O)_2(SbW_{10}O_{37})(SbW_8O_{31})\}_2]^{22-}$ species. Before the analyses of each measurement, the contribution of the capillaries and the solvent was subtracted using a reference containing the solvent according to standard procedures.

The experimental scattering data were compared to simulated scattering ones calculated on the basis of the structural parameters of the related compounds using the CIF files obtained after the single-crystal X-ray diffraction analyses. The simulated scattering curves were computed by using the SolX software.[38–40]

Luminescence measurements

Luminescent measurements were performed on an Edinburgh Instruments FLSP920 UV-vis-NIR spectrometer setup. A 450 W xenon lamp was used as steady-state excitation source. Time-resolved measurements were recorded using a 60 W pulsed xenon lamp operating at a frequency of 100 Hz. A Hamamatsu R5509-72 photomultiplier tube was used to detect emission in the NIR region. All luminescence measurements were recorded at room temperature. Crystalline powdered samples of compounds **5** and **7** were put between quartz plates (Starna cuvettes for powder samples, type 20/C/Q/0.2).

Inductively coupled plasma spectroscopy

Crystals of compound **1**–**8** were dissolved in 2% HNO_3 solutions and were analyzed using a Vista-Pro Varian ICP-OES. Each compound was analyzed separately to determine the Na / Sb

/ W / Ln (Ln = Gd, Tb, Dy, Ho, Er, Tm, Yb, Lu) ratios. Based on the number of W atoms in each compound, the percentages of each element can be estimated.

Infrared spectroscopy

Infrared spectra of the compounds **1-8** (see Supplementary information) were measured on a Perkin Elmer Spectrum Two™ spectrometer between 4000 and 400 cm^{-1}, equipped with a diamond Attenuated Total Reflectance (ATR) accessory. Spectra are shown in Figure S2. No ATR correction was performed on the IR spectra.

SEM/EDS and optical microscope photographs

Scanning electronic microscopy images of the crystals of the compounds are shown in Figure S3. Photographs of the crystals were performed on a HITACHI S3400N SEM equipped with a tungsten filament as well as on a binocular optical microscope.

Thermogravimetric analysis

Thermogravimetric (TG) experiments have been carried out for compounds **1-8**, on a thermoanalyzer TGA 92 SETARAM under air atmosphere with a heating rate of 1°C.min^{-1} from room temperature up to 800°C. The TG curves are shown in Figure S4.

Supplementary informations. Crystal data and structure refinement parameters for compounds **1-8** (Table S1), BVS calculations of the Sb atoms in the $\{Sb_3O_7\}$ unit (Table S2), IR wavenumbers (in cm^{-1}) of the polyanionic backbone in $Na_9[SbW_9O_{33}]\cdot 12H_2O$, $(N(CH_3)_4)_{10}Na_{12}[Sb_8W_{36}O_{132}(H_2O)_4]\cdot 72H_2O$ and, in compounds **1-8** (Table S3), micrographs of crystals of compounds **1-8** (Figure S1), TGA curves for compounds **1-8** (Figure S2), IR spectra of compounds **1-8** and comparison with $Na_9[SbW_9O_{33}]\cdot 12H_2O$ and $(N(CH_3)_4)_{10}Na_{12}[Sb_8W_{36}O_{132}(H_2O)_4]\cdot 72H_2O$ in the region 4000-400 cm^{-1} and 1100-400 cm^{-1} (Figure S3). Crystallographic data for: compound **1** (CIF) CCDC 2012023, compound **2** (CIF) CCDC 2012022, compound **3** (CIF) CCDC 2012024, compound **4** (CIF) CCDC 2012027, compound 5 **(**CIF) CCDC 2012021, compound **6** (CIF) CCDC 2012025, compound **7** (CIF) CCDC 2012028, compound **8** (CIF) CCDC 2012026.

Acknowledgment:

The authors would like to thank Mrs. Nora Djelal for her technical assistance with the SEM images and TG measurements (UCCS). Chevreul Institute (FR 2638), Ministère de l'Enseignement Supérieur, de la Recherche et de l'Innovation, Hauts-de-France Region and FEDER are acknowledged for supporting and funding partially this work. M.D. and S.D. would like to thank the ANR (French National Agency for Research) for the funding of the JCJC POMAR project. D.M and R.V.D acknowledge Ghent University for a BOF PhD grant (BOF15/24J/049).

[1] M. T. Pope, Y. Jeannin, M. Fournier, *Heteropoly and Isopoly Oxometalates*, Springer Berlin, Berlin, **2013**.

[2] M. T. Pope, A. Müller, *Angew. Chem. Int. Ed.* **1991**, *30*, 34–48.

[3] M. T. Pope, A. Müller, Eds. , *Polyoxometalates: From Platonic Solids to Anti-Retroviral Activity*, Springer Netherlands, Dordrecht, **1994**.

[4] C. L. Hill, *Chem. Rev.* **1998**, *98*, 1–390.

[5] D.-L. Long, R. Tsunashima, L. Cronin, *Angew. Chem. Int. Ed.* **2010**, *49*, 1736–1758.

[6] A. Proust, B. Matt, R. Villanneau, G. Guillemot, P. Gouzerh, G. Izzet, *Chem. Soc. Rev.* **2012**, *41*, 7605–7622.

[7] M. T. Pope, U. Kortz, *Encyclopedia of Inorganic and Bioinorganic Chemistry*, **2011**.

[8] O. Oms, A. Dolbecq, P. Mialane, *Chem. Soc. Rev.* **2012**, *41*, 7497–7536.

[9] A. Dolbecq, E. Dumas, C. R. Mayer, P. Mialane, *Chem. Rev.* **2010**, *110*, 6009–6048.

[10] M. Leyrie, G. Hervé, *Nouv. J. Chim.* **1978**, *2*, 223–227.

[11] R. Contant, A. Teze, *Inorg. Chem.* **1985**, *24*, 4610–4614.

[12] S. S. Mal, M. H. Dickman, U. Kortz, *Chem. Eur. J.* **2008**, *14*, 9851–9855.

[13] M. H. Dickman, G. J. Gama, K.-C. Kim, M. T. Pope, *J Clust Sci* **1996**, *7*, 567–583.

[14] V. S. Korenev, P. A. Abramov, A. L. Gushchin, D. V. Stass, V. M. Babaev, I. Kh. Rizvanov, M. N. Sokolov, *Russ. J. Inorg. Chem.* **2019**, *64*, 1105–1114.

[15] M. Dufaye, S. Duval, G. Stoclet, X. Trivelli, M. Huvé, A. Moissette, T. Loiseau, *Inorg. Chem.* **2019**, *58*, 1091–1099.

[16] M. Dufaye, S. Duval, T. Loiseau, *CrystEngComm* **2020**, *22*, 3549–3562.

[17] H. El Moll, B. Nohra, P. Mialane, J. Marrot, N. Dupré, B. Riflade, M. Malacria, S. Thorimbert, B. Hasenknopf, E. Lacôte, P. A. Aparicio, X. López, J. M. Poblet, A. Dolbecq, *Chem. Eur. J.* **2011**, *17*, 14129–14138.

[18] M. Mirzaei, H. Eshtiagh-Hosseini, N. Lotfian, A. Salimi, A. Bauzá, R. Van Deun, R. Decadt, M. Barceló-Oliver, A. Frontera, *Dalton Trans.* **2014**, *43*, 1906–1916.

[19] M. Zimmermann, N. Belai, R. J. Butcher, M. T. Pope, E. V. Chubarova, M. H. Dickman, U. Kortz, *Inorg. Chem.* **2007**, *46*, 1737–1740.

[20] B. S. Bassil, M. H. Dickman, I. Römer, B. von der Kammer, U. Kortz, *Angew. Chem. Int. Ed.* **2007**, *46*, 6192–6195.

[21] K. Wassermann, M. H. Dickman, M. T. Pope, *Angew. Chem. Int. Ed. Engl.* **1997**, *36*, 1445–1448.

[22] F. Hussain, F. Conrad, G. Patzke, *Angew. Chem. Int. Ed.* **2009**, *48*, 9088–9091.

[23] F. Hussain, B. Spingler, F. Conrad, M. Speldrich, P. Kögerler, C. Boskovic, G. R. Patzke, *Dalton Trans.* **2009**, 4423.

[24] F. Hussain, G. R. Patzke, *CrystEngComm* **2011**, *13*, 530–536.

[25] K. Fukaya, T. Yamase, *Angew. Chem. Int. Ed.* **2003**, *42*, 654–658.

[26] X. Fang, T. M. Anderson, C. Benelli, C. L. Hill, *Chem. Eur. J.* **2005**, *11*, 712–718.

[27] B. S. Bassil, U. Kortz, *Z. anorg. allg. Chem.* **2010**, *636*, 2222–2231.

[28] L.-L. Li, H.-Y. Han, Y.-H. Wang, H.-Q. Tan, H.-Y. Zang, Y.-G. Li, *Dalton Trans.* **2015**, *44*, 11429–11436.

[29] M. Dufaye, S. Duval, B. Hirsou, G. Stoclet, T. Loiseau, *CrystEngComm* **2018**, *20*, 5500–5509.

[30] S. Yao, J.-H. Yan, H. Duan, Q.-Q. Jia, Z.-M. Zhang, E.-B. Wang, *RSC Adv.* **2015**, *5*, 76206–76210.

[31] R. D. Shannon, *Acta Cryst A* **1976**, *32*, 751–767.

[32] M. Nyman, *Coord. Chem. Rev.* **2017**, *352*, 461–472.

[33] M. Bösing, I. Loose, H. Pohlmann, B. Krebs, *Chem. Eur. J.* **1997**, *3*, 1232–1237.

[34] *Brucker Analytical X-ray Systems: Madison, WI, 2008* **2014**.

[35] G. M. Sheldrick, *Brucker-Siemens Area detector Absorption and Other Correction* **2015b**.

[36] G. M. Sheldrick, *Acta Crystallographica Section A Foundations of Crystallography* **2008**, *64*, 112–122.

[37] O. V. Dolomanov, L. J. Bourhis, R. J. Gildea, J. A. K. Howard, H. Puschmann, *J. Appl. Crystallogr.* **2009**, *42*, 339–341.

[38] X. Zuo, G. Cui, K. M. Merz, L. Zhang, F. D. Lewis, D. M. Tiede, *Proc. Natl. Acad. Sci.* **2006**, *103*, 3534–3539.

[39] J. L. O'Donnell, X. Zuo, A. J. Goshe, L. Sarkisov, R. Q. Snurr, J. T. Hupp, D. M. Tiede, *J. Am. Chem. Soc.* **2007**, *129*, 1578–1585.

[40] F. Förster, B. Webb, K. A. Krukenberg, H. Tsuruta, D. A. Agard, A. Sali, *J. Mol. Biol.* **2008**, *382*, 1089–1106.